JACS
JOURNAL OF THE AMERICAN CHEMICAL SOCIETY

ARTICLE

pubs.acs.org/JACS

Noncovalent Ligand-to-Ligand Interactions Alter Sense of Optical Chirality in Luminescent Tris(β-diketonate) Lanthanide(III) Complexes Containing a Chiral Bis(oxazolinyl) Pyridine Ligand

Junpei Yuasa,* Tomoko Ohno, Kohei Miyata,† Hiroyuki Tsumatori, Yasuchika Hasegawa,† and Tsuyoshi Kawai*

Graduate School of Materials Science, Nara Institute of Science and Technology, 8916-5 Takayama, Ikoma, Nara 630-0192, Japan

Supporting Information

ABSTRACT: Highly luminescent tris[β-diketonate (HFA, 1,1,1,5,5,5-hexafluoropentane-2,4-dione)] europium(III) complexes containing a chiral bis(oxazolinyl) pyridine (pybox) ligand—[(Eu^{III}(*R*)-Ph-pybox)$(HFA)_3$], [(Eu^{III}(*R*)-*i*-Pr-pybox)$(HFA)_3$], and [(Eu^{III}(*R*)-Me-Ph-pybox)$(HFA)_3$])—exhibit strong circularly polarized luminescence (CPL) at the magnetic-dipole ($^5D_0 \rightarrow {}^7F_1$) transition, where the [(Eu^{III}(*R*)-Ph-pybox)$(HFA)_3$] complexes show virtually opposite CPL spectra as compared to those with the same chirality of [(Eu^{III}(*R*)-*i*-Pr-pybox)$(HFA)_3$] and [(Eu^{III}(*R*)-Me-Ph-pybox)$(HFA)_3$]. Similarly, the [(Tb^{III}(*R*)-Ph-pybox)$(HFA)_3$] complexes were found to exhibit CPL signals almost opposite to those of [(Tb^{III}(*R*)-*i*-Pr-pybox)$(HFA)_3$] and [(Tb^{III}(*R*)-Me-Ph-pybox)$(HFA)_3$] complexes with the same pybox chirality. Single-crystal X-ray structural analysis revealed ligand−ligand interactions between the pybox ligand and the HFA ligand in each lanthanide(III) complex: π−π stacking interactions in the Eu^{III} and Tb^{III} complexes with the Ph-pybox ligand, CH/F interactions in those with the *i*-Pr-pybox ligand, and CH/π interactions in those with the Me-Ph-pybox ligand. The ligand−ligand interactions between the achiral HFA ligands and the chiral pybox results in an asymmetric arrangement of three HFA ligands around the metal center. The metal center geometry varies depending on the types of ligand−ligand interaction.

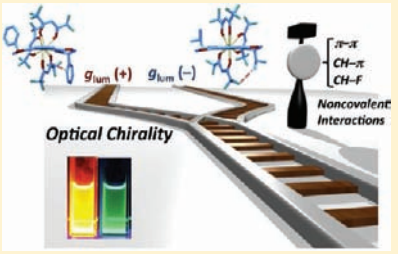

INTRODUCTION

Control of chirality around a metal center of complexes is an important element in achieving a highly enantioselective catalytic reaction[1−5] and in developing a chiroptical probe.[6−8] The metal center chirality is basically induced by chirality of the host ligand, which is often transferred to the coordination structure and thus chirality of guest ligands through noncovalent ligand-to-ligand interactions in addition to the coordination bonding (Scheme 1).[2−5,9−12] Because of such complicated ligand effects, the systematic evaluation and programming of the sense of chirality around the metal center remains challenging.[2−5,9−12] In the luminecent metal complexes, such complicated ligand field structure is sensitively reflected in the sign and magnitude of circularly polarized luminescence (CPL),[13−16] and therefore the CPL technique is often used as an indicator of the chirality at the metal center.[17−25] In this viewpoint, systematic comparison of chiral structural information from CPL measurements with absolute configuration determined by X-ray crystallographic analysis could bring a clearer understanding of the molecular mechanisms responsible for determining the sense of optical chirality at the metal center.

Herein we report that noncovalent ligand-to-ligand interactions alter the sense of optical chirality in luminescent tris(β-diketonate) europium(III) and terbium(III) complexes containing chiral bis(oxazolinyl) pyridine ligands (Ph-, *i*-Pr-, and Me-Ph-pybox). Luminescence from lanthanide(III) complexes often showed large

Scheme 1

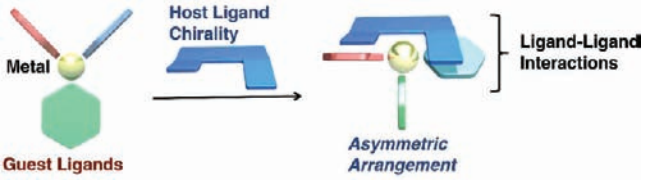

circular polarization due to their magnetic and electronic dipole transition nature.[13−16] Bis(oxazoline) ligands have been extensively utilized in asymmetric synthesis of a variety of valuable chiral compounds,[1,2,26,27] while lanthanide(III) β-diketonate complexes have been exploited for applications as highly luminescent materials.[28,29] In this study, we used X-ray crystallography to successfully determine absolute configuration around each metal center. This is the first time extensive analysis on investigation of opposite sense of chirality in luminescent metal complexes based on CPL methods has been combined with X-ray crystallographic analysis, providing valuable insight into how the chiral host ligand (pybox) determines the sense of optical chirality at the metal center.

Received: March 15, 2011
Published: May 20, 2011

EXPERIMENTAL SECTION

Materials. (*R*,*R*/*S*,*S*)-2,6-Bis(4-phenyl-2-oxazolin-2-yl)pyridine [(*R*/*S*)-Ph-pybox] and (*R*,*R*/*S*,*S*)-2,6-bis(4-isopropyl-2-oxazolin-2-yl)pyridine [(*R*/*S*)-*i*-Pr-pybox] were purchased from Tokyo Chemical Industry Co., Ltd. 2,6-Bis[(4*R*,5*R*/4*S*,5*S*)-4,5-dihydro-4-methyl-5-phenyl-2-oxazolyl]pyridine [(*R*/*S*)-Me-Ph-pybox] and [$^2H_3$]acetonitrile (CD_3CN) used as solvent were obtained from Aldrich. Tris(β-diketonate) europium(III) and terbium(III) ($[Eu^{III}(HFA)_3(H_2O)_2]$ and $[Tb^{III}(HFA)_3(H_2O)_2]$, respectively) were prepared by the procedure described in a previous report.[28] Tris[β-diketonate (HFA, 1,1,1,5,5,5-hexafluoropentane-2,4-dione)] europium(III) and terbium(III) complexes containing a chiral bis(oxazolinyl) pyridine ligand (Ph-, Me-Ph-, and *i*-Pr-pybox) were synthesized as follows. For $[(Eu^{III}(R)$-*i*-Pr-pybox$)(HFA)_3]$, $[Eu^{III}(HFA)_3]$ (650 mg, 0.74 mmol) and (*R*)-*i*-Pr-pybox (210 mg, 0.69 mmol) were dissolved in methanol (20 mL) and refluxed under stirring for 8 h. The reaction solution was evaporated in a rotary evaporator. The obtained powder was recrystallized from a methanol solution (yield 59%). HRMS [ESI-MS (positive)]: *m*/*z* calcd for $C_{27}H_{25}EuF_{12}N_3O_6$ ($[M - HFA]^+$), 868.076 63; found, 868.077 07. $[(Eu^{III}(R)$-Ph-pybox$)(HFA)_3]$ and $[(Tb^{III}(R)$-Ph-pybox$)(HFA)_3]$ were synthesized by the same procedure as $[(Eu^{III}(R)$-*i*-Pr-pybox$)(HFA)_3]$. For the synthesis of $[(Eu^{III}(R)$-Me-Ph-pybox$)(HFA)_3]$, $[(Tb^{III}(R)$-*i*-Pr-pybox$)(HFA)_3]$, and $[(Tb^{III}(R)$-Me-Ph-pybox$)(HFA)_3]$, acetonitrile was used instead of methanol to dissolve (*R*)-Me-Ph-pybox. $[(Eu^{III}(R)$-Ph-pybox$)(HFA)_3]$, HRMS [ESI-MS (positive)]: *m*/*z* calcd for $C_{33}H_{21}EuF_{12}N_3O_6$ ($[M - +HFA]^+$), 936.045 42; found, 936.044 66. $[(Eu^{III}(R)$-Me-Ph-pybox$)(HFA)_3]$, HRMS [ESI-MS (positive)]: *m*/*z* calcd for $C_{35}H_{25}EuF_{12}N_3O_6$ ($[M - HFA]^+$), 964.076 75; found, 964.076 81. $[(Tb^{III}(R)$-Ph-pybox$)(HFA)_3]$, HRMS [ESI-MS (positive)]: *m*/*z* calcd for $C_{33}H_{21}F_{12}N_3O_6Tb^+$ ($[M - HFA]^+$), 942.049 22; found, 942.049 01. $[(Tb^{III}(R)$-*i*-Pr-pybox$)(HFA)_3]$, HRMS [ESI-MS (positive)]: *m*/*z* calcd for $C_{27}H_{25}F_{12}N_3O_6Tb^+$, 874.080 52; found, 874.080 60. $[(Tb^{III}(R)$-Me-Ph-pybox$)(HFA)_3]$, HRMS [ESI-MS (positive)]: *m*/*z* calcd for $C_{35}H_{25}F_{12}N_3O_6Tb^+$, 970.080 52; found, 970.080 62. The (*S*)-isomers of the Eu^{III} and Tb^{III} complexes were prepared by the same procedure as those of the (*R*)-isomers.

Spectral Measurements. Emission quantum yields of the Eu^{III} and Tb^{III} complexes (1.0×10^{-2} M) were measured on a calibrated integrating sphere system in CD_3CN at 298 K. In the emission lifetime measurements, the samples were excited by a N_2 laser (Usho KEC-160; wavelength 337 nm; pulse width 600 ps; 10 Hz). The emission profiles were recorded with a streak camera (Hamamatsu, picosecond fluorescence measurement system, C4780). Measurement of absorption and CD spectra were performed at room temperature on Jasco V-660, Jasco J-725, and Jasco J-820 instruments. The emission spectra were measured at room temperature on a Jasco FP-6500 instrument. A schematic diagram of the CPL measurement system used in this study is given in Scheme S1 in Supporting Information.[30]

Crystallography. Suitable crystals for single-crystal X-ray structural analysis were grown by slow evaporation of methanol solutions of the Eu^{III} and Tb^{III} complexes. Single crystals of Eu^{III} and Tb^{III} complexes were mounted with epoxy resin on a glass fiber. X-ray diffraction intensity was collected with a Rigaku Raxis Rapid (3 kW) imaging plate area detector with graphite monochromated Mo Kα radiation at 153 K. All calculations were performed with the Rigaku CrystalStructure 3.8.1 software. Computation of molecular graphics was performed with ORTEP-3 for Windows.

RESULTS AND DISCUSSION

Opposite Sign in CPL and CD Spectra of the Eu^{III} and Tb^{III} Complexes. Figure 1a−d show the circularly polarized luminescence (CPL) and emission spectra of CD_3CN solutions of tris[β-diketonate (HFA, 1,1,1,5,5,5-hexafluoropentane-2,4-dione)] Eu^{III} complexes with each optical isomer of the pybox ligands [(*S*)- and (*R*)-isomers of Ph-, *i*-Pr-, and Me-Ph-pybox] in the spectral range of the $^5D_0 \rightarrow {}^7F_1$ and $^5D_0 \rightarrow {}^7F_2$ transitions, which are magnetic and electronic-dipole transitions, respectively.[31] The magnetic dipole transition satisfies the magnetic-dipole selection rule, $\Delta J = 0, \pm 1$ (except $0 \leftrightarrow 0$), which often shows particularly large circular polarization.[13−16] Almost complete mirror-image CPL signals are obtained for the Eu^{III} complexes with their enantiomer pairs, where the CPL spectra are normalized with respect to the $^5D_0 \rightarrow {}^7F_1$ transitions (Figure 1a−c). Similarly, tris(HFA) Tb^{III} complexes with each optical isomer of the pybox ligands exhibit strong CPL at the $^5D_4 \rightarrow {}^7F_5$ transition, where their CPL spectra are in mirror image to each other (Figure 1e−g). The luminescence dissymmetry factors (g_{lum}) of the Eu^{III} and Tb^{III} complexes are summarized in Table 1 together with their emission quantum yields (ϕ_{f-f}).

Dissymmetry factor is defined as $g_{lum} = 2(I_L - I_R)/(I_L + I_R)$, where I_L and I_R refer to the intensity of left and right circularly polarized light, respectively. All of the Eu^{III} complexes examined here exhibit relatively intense CPL activity and high emission quantum yields. Among them, $[(Eu^{III}(R)$-*i*-Pr-pybox$)(HFA)_3]$ shows the largest $|g_{lum}|$ value (0.46) as well as the highest emission quantum yield (41%) (Table 1). High emission quantum yields of the Eu^{III} complexes seem to be due to effective suppression of the nonradiative transition via vibrational relaxation in the Eu^{III} complexes with the HFA ligands.[28,29,32] In order to clarify this effect, we have estimated radiative (k_r) and nonradiative (k_{nr}) rate constants of the Eu^{III} complexes from the emission lifetimes (τ_{obs}) and the emission quantum yields as summarized in Table 1 (for emission decay profiles of the Eu^{III} complexes, see Supporting Information, Figure S2). The relatively small nonradiative rate constants [$k_{nr} = (4.8-5.4) \times 10^2$ s^{-1}] suggest the effective suppression of the nonradiative transition through the vibrational relaxation processes in the present Eu^{III} complexes.[32] Conversely, the Tb^{III} complexes also possess relatively strong CPL activity ($|g_{lum}| = 0.044-0.082$); however, their emission lifetimes ($\tau_{obs} = 2.1 \times 10^{-3}$ to 1.2×10^{-2} ms) are much shorter than those of the Eu^{III} complexes ($\tau_{obs} = 1.22-1.27$ ms) (Table 1). In the Tb^{III} complexes having HFA ligands, nonradiative deactivation of the terbium emission through a back-energy transfer process [$T_1 \leftarrow Tb(^5D_4)$] is a common quenching process,[33,34] because the triplet state of HFA ligand (22 200 cm^{-1}) is much closer to the emitting level of Tb(III) ion (20 500 cm^{-1}).[35] In fact, the emission of $[(Tb^{III}(R)$-Ph-pybox$)(HFA)_3]$ exhibits a remarkable temperature dependence showing a continuously decreasing intensity with increasing the temperature, indicating the back-energy transfer process [$T_1 \leftarrow Tb(^5D_4)$] (see Supporting Information, Figure S3).[33]

On the other hand, strong CPL activities of the Eu^{III} and Tb^{III} complexes indicate that induced chirality of HFA ligands surrounding the metal center contributes to the sign and magnitude of the CPL. The circular dichroism (CD) spectra of the Eu^{III} and Tb^{III} complexes reveal strong CD bands in the spectral range of the $\pi-\pi^*$ transition of the HFA ligands, suggesting the induced chirality in the HFA ligands by pybox through coordination to the lanthanide(III) [Ln^{III}] metal centers (Figure 2). In the CPL spectra, the sign of the CPL for $[(Eu^{III}(R)$-Ph-pybox$)(HFA)_3]$ follows the sequence +, − at the $^5D_0 \rightarrow {}^7F_1$ and $^5D_0 \rightarrow {}^7F_2$ transitions (Figure 1a, dark red line), which is reversed to −, + sign sequence for $[(Eu^{III}(R)$-*i*-Pr-pybox$)(HFA)_3]$ and $[(Eu^{III}(R)$-Me-Ph-pybox$)(HFA)_3]$ (Figure 1b and c, dark red lines, respectively). Similarly, the CD spectrum of $[(Eu^{III}(R)$-Ph-pybox$)(HFA)_3]$ in the wavelength range around 230−360 nm at the $\pi-\pi^*$ transition of the HFA ligands (Figure 2a,

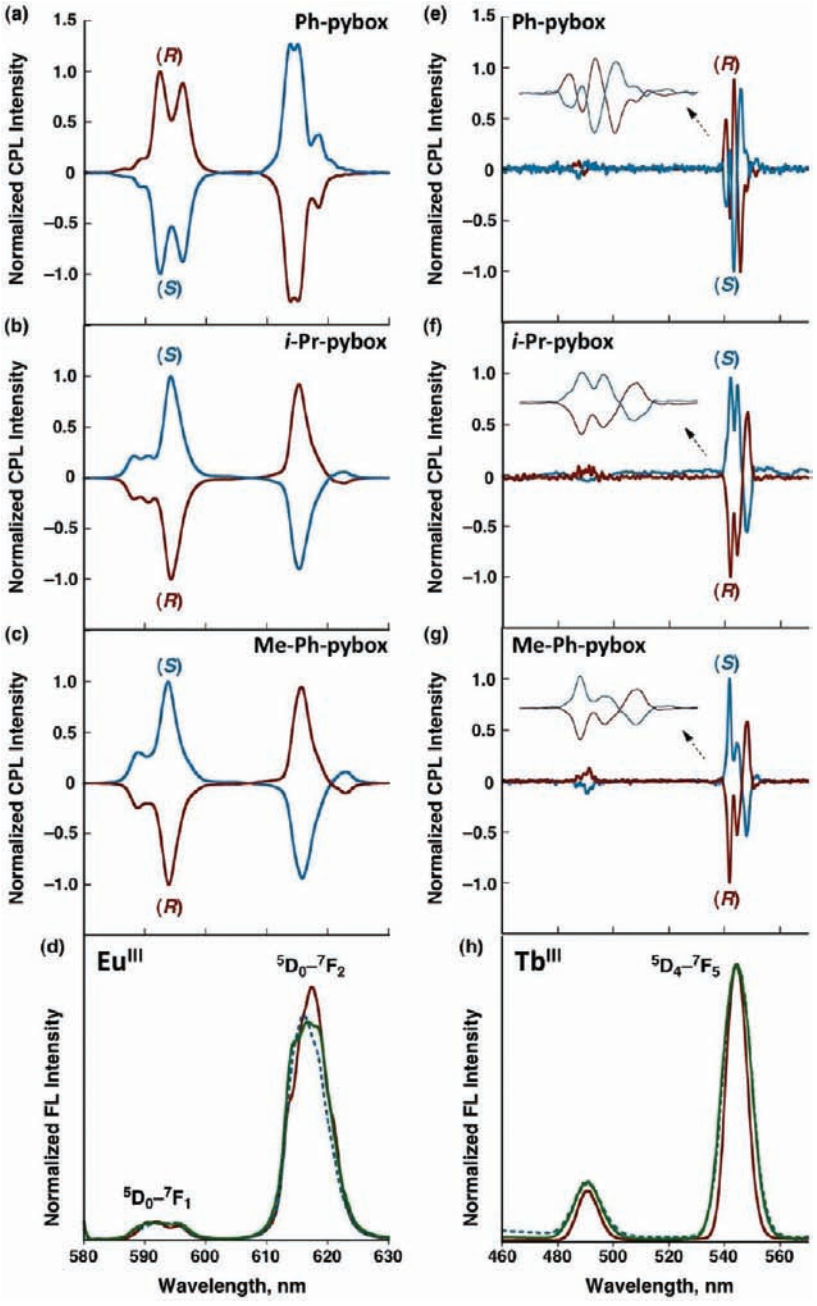

Figure 1. Dark red lines show normalized CPL spectra of CD_3CN solutions (1.0×10^{-2} M) of (a) [(Eu^{III}(*R*)-Ph-pybox)$(HFA)_3$], (b) [(Eu^{III}(*R*)-*i*-Pr-pybox)$(HFA)_3$], (c) [(Eu^{III}(*R*)-Me-Ph-pybox)$(HFA)_3$], (e) [(Tb^{III}(*R*)-Ph-pybox)$(HFA)_3$], (f) [(Tb^{III}(*R*)-*i*-Pr-pybox)$(HFA)_3$], and (g) [(Tb^{III}(*R*)-Me-Ph-pybox)$(HFA)_3$] at 298 K. Excitation wavelength λ = 375 nm. Blue lines show those of their optical isomers [(*S*)-isomers]. (d) Normalized emission spectra of [(Eu^{III}(*R*)-Ph-pybox)$(HFA)_3$] (dark red solid line) [4.4×10^{-5} M], [(Eu^{III}(*R*)-*i*-Pr-pybox)$(HFA)_3$] (blue dashed line) [3.1×10^{-5} M], and [(Eu^{III}(*R*)-Me-Ph-pybox)$(HFA)_3$] (green solid line) [2.8×10^{-5} M] in CD_3CN at 298 K. Excitation wavelength λ = 360 nm. (h) Normalized emission spectra of [(Tb^{III}(*R*)-Ph-pybox)$(HFA)_3$] (dark red solid line) [4.4×10^{-5} M], [(Tb^{III}(*R*)-*i*-Pr-pybox)$(HFA)_3$] (blue dashed line) [3.1×10^{-5} M], and [(Tb^{III}(*R*)-Me-Ph-pybox)$(HFA)_3$] (green solid line) [2.8×10^{-5} M] in CD_3CN at 298 K. Excitation wavelength λ = 350 nm. Emission and CPL spectra are normalized with respect to (a–d) $^5D_0 \rightarrow {}^7F_1$ transition and (e–h) $^5D_4 \rightarrow {}^7F_5$ transition.

dark red line) shows a quasi mirror image of the CD patterns of [(Eu^{III}(*R*)-*i*-Pr-pybox)$(HFA)_3$] and [(Eu^{III}(*R*)-Me-Ph-pybox)-$(HFA)_3$] (Figure 2b and c, dark red lines, respectively).[36−39] A similar sign inversion of CPL and CD spectra is observed in the Tb^{III} complexes, where [(Tb^{III}(*R*)-Ph-pybox)$(HFA)_3$] complex exhibits CPL and CD signals (dark red lines in Figures 1e and 2e, respectively) nearly opposite to those of [(Tb^{III}(*R*)-*i*-Pr-pybox)$(HFA)_3$] and [(Tb^{III}(*R*)-Me-Ph-pybox)$(HFA)_3$] having the same chirality of the pybox ligands (dark red lines in Figures 1f,g and 2f,g).[40] These results indicate that (*R*)-Ph-pybox plays an opposite role to those of [(Ln^{III}(*R*)-*i*-Pr-pybox)-$(HFA)_3$] and [(Ln^{III}(*R*)-Me-Ph-pybox)$(HFA)_3$] in the chiral discrimination of the three HFA ligands surrounding the metal center of [(Ln^{III}(*R*)-Ph-pybox)$(HFA)_3$].

dx.doi.org/10.1021/ja201984u |*J. Am. Chem. Soc.* 2011, 133, 9892–9902

Table 1. Emission Quantum Yields, Dissymmetry Factors of CPL Spectra for Three Transitions, Emission Lifetimes, Radiative and Nonradiative Rates, and Coordination Geometries of Eu^{III} and Tb^{III} Complexes

		g_{lum}[b]						
complex	ϕ_{f-f}[a] (%)	$^5D_0 \rightarrow {}^7F_1$	$^5D_0 \rightarrow {}^7F_2$	$^5D_4 \rightarrow {}^7F_5$	τ_{obs}[c] (ms)	k_r[d] (s^{-1})	k_{nr}[e] (s^{-1})	coord geom[f]
[(Eu^{III}(*R*)-Ph-pybox) ($HFA)_3$]	34	0.15	−0.020		1.22 (1.22)[g]	2.8×10^2	5.4×10^2	I
[(Eu^{III}(*R*)-*i*-Pr-pybox) ($HFA)_3$]	41	−0.46	0.034		1.24 (1.19)[g]	3.3×10^2	4.8×10^2	IV
[(Eu^{III}(*R*)-Me-Ph-pybox) ($HFA)_3$]	39	−0.35	0.026		1.27 (1.32)[g]	3.1×10^2	4.8×10^2	III
[(Tb^{III}(*S*)-Ph-pybox) ($HFA)_3$]	[h]			−0.045 (540 nm)	1.2×10^{-2} (1.2×10^{-2})[i]			II
[(Tb^{III}(*S*)-*i*-Pr-pybox) ($HFA)_3$]	[h]			0.044 (542 nm)	2.1×10^{-3} (2.0×10^{-3})[i]			V
[(Tb^{III}(*S*)-Me-Ph-pybox) ($HFA)_3$]	[h]			0.082 (542 nm)	3.5×10^{-3} (3.4×10^{-3})[i]			IV

[a] Emission quantum yields (ϕ_{f-f}) of Eu^{III} complexes in CD_3CN (1.0×10^{-2} M) were measured by excitation at 465 nm ($^7F_0 \rightarrow {}^5D_2$). [b] CPL signals are given by the difference between the left and right circularly polarized emission intensities ($I_{CPL} = I_L - I_R$). [c] Emission lifetimes (τ_{obs}) were measured by excitation at 337 nm. [d] Radiative rate is given by $k_r = \phi_{f-f}/\tau_{obs}$. [e] Nonradiative rate is given by $k_{nr} = 1/\tau_{obs} - k_r$. [f] Definition of the sense of chiral arrangement of HFA ligands is given in the caption of Figure 5. [g] Values in parentheses denote emission lifetimes (τ_{obs}) of the (*S*)-isomers of the Eu^{III} complex. [h] Too small to be determined accurately. [i] Values in parentheses denote emission lifetimes (τ_{obs}) of the (*R*)-isomers of the Tb^{III} complex.

Single-Crystal X-ray Structural Analysis of Eu^{III} and Tb^{III} Complexes. In order to understand how pybox ligands determine the sense of optical chirality at the metal center, we have determined the absolute configuration around the metal centers by using X-ray crystallographic analysis. Suitable crystals were grown by slow evaporation of methanol solutions of both the Eu^{III} and Tb^{III} complexes. The crystallographic data for the Eu^{III} and Tb^{III} complexes are summarized in Tables 2 and 3, respectively. X-ray crystallography reveals ligand−ligand interactions between the pybox ligands and the HFA ligands in each lanthanide(III) complex. For Eu^{III} complexes having (*R*)-pybox ligands one can see $\pi-\pi$ stacking interaction ($d_{\pi/\pi}$ = 3.463 Å, C26···Ph1 distance) in [(Eu^{III}(*R*)-Ph-pybox)-($HFA)_3$]; CH/F interaction ($d_{CH/F}$ = 2.665 Å, H20···F17 distance) in [(Eu^{III}(*R*)-*i*-Pr-pybox)($HFA)_3$]; and CH/π interaction ($d_{CH/\pi}$ = 2.807 Å, H2···C27 distance) in [(Eu^{III}(*R*)-Me-Ph-pybox)($HFA)_3$] (Figure 3a−c, respectively). For Tb^{III} complexes with (*S*)-pybox ligands, one can see $\pi-\pi$ stacking interaction ($d_{\pi/\pi}$ = 3.447 Å, C36···Ph2 distance) in [(Tb^{III}(*S*)-Ph-pybox)($HFA)_3$]; CH/F interactions ($d_{CH/F}$ = 2.863 Å, H6···F15 distance; $d_{CH/F}$ = 2.599 Å, H18···F6 distance) in [(Tb^{III}(*S*)-*i*-Pr-pybox)($HFA)_3$]; and CH/π interaction ($d_{CH/\pi}$ = 2.739 Å, H23···C39 distance) in [(Tb^{III}(*S*)-Me-Ph-pybox)($HFA)_3$] (Figure 3d−f, respectively).[41,42] In the case of lanthanide(III) complexes with Ph- and Me-Ph-pybox ligands ([(Ln^{III}-Ph-pybox)($HFA)_3$] and [(Ln^{III}-Me-Ph-pybox)-($HFA)_3$], respectively), Ph and Me groups of pybox ligands are bound to the HFA π-plane (Figure 3a,c,d,f bottom). Conversely, the *i*-Pr group of *i*-Pr-pybox interacts with the distal CF_3 group of the HFA ligand in [(Eu^{III}(*R*)-*i*-Pr-pybox)($HFA)_3$] and [(Tb^{III}(*S*)-*i*-Pr-pybox)($HFA)_3$] (Figure 3b,e bottom). It should be noted that both Me groups of the (*S*)-Me-Ph-pybox ligand interact with HFA ligands in the [(Tb^{III}(*S*)-*i*-Pr-pybox)($HFA)_3$] complex (Figure 3e), although only one side arm of the pybox ligand is attached to the HFA ligand in the other lanthanide(III) complexes (Figure 3a−d,f).

In contrast to the ligand−ligand interactions within the complex, there is no appreciable intermolecular interaction between the lanthanide(III) complexes in the molecular packing diagrams. Thus, crystal structures of the Eu^{III} and Tb^{III} complexes (Figure 3) should reflect the average arrangement of the HFA ligands for the complexes in solution, albeit crystal-packing effects on one hand and solvation effects on the other hand somewhat influence the coordination of the complexes.[40,43−45]

The ligand−ligand interaction between the one side arm of the pybox ligand and the HFA ligand should differentiate two side arms of each pybox ligand, inducing discrimination of the three HFA ligands surrounding the metal center (vide infra).[46,47] Top views of the crystal structures of the Eu^{III} and Tb^{III} complexes are shown in Figure 4, where individual side arms are distinguished by red (Ph1, *i*-Pr1, and Me1) and blue (Ph2, *i*-Pr2, and Me2). Except in the [(Tb^{III}(*S*)-*i*-Pr-pybox)($HFA)_3$] case (Figure 4h), Ph2, *i*-Pr2, and Me2 side arms have no appreciable molecular interaction with the HFA ligands, whereas Ph1, *i*-Pr1, and Me1 side arms are attached to HFA ligands (denoted as A) by $\pi-\pi$ stacking, CH/F, and CH/π interactions, respectively (vide supra). These ligand−ligand interactions cause in plane strain and ring bending of pybox ligands [specifically (*R*)- and (*S*)-Ph-pybox ligands in Figure 4panels c and g, respectively], making a distinction between inside and outside of the ligand faces. Similarly, three HFA ligands surrounding the metal center possess a different stereochemical environment; one (denoted as A) interacts with the side arms of the pybox ligand (Ph1, *i*-Pr1, and Me1) while the others (denoted as B and C) have no specific interaction with the pybox ligand (except [(Tb^{III}(*S*)-*i*-Pr-pybox)($HFA)_3$], Figure 4h). Core structures of [(Eu^{III}(*S*)-*i*-Pr-pybox)($HFA)_3$] and [(Eu^{III}(*R*)-*i*-Pr-pybox)($HFA)_3$] around the Eu^{III} metal center are shown in the middle of Figure 4panels a and b, respectively, in which individual HFA ligands are distinguished (A−C). These core structures are nonsuperimposable images of each other. Mirror-image arrangement is also found in core structures of [(Tb^{III}(*R*)-Me-Ph-pybox)($HFA)_3$] and [(Tb^{III}(*S*)-Me-Ph-pybox)($HFA)_3$] (middle of Figure 4panels e and f, respectively). Such mirror symmetry breaking in the coordination geometries of HFA ligands around the metal center should be responsible for the induced circular dichroism (ICD) and the strong CPL activity of the Eu^{III} and Tb^{III} complexes (Figures 1 and 2, respectively), Thus, we focused on coordination structures of HFA ligands at the metal centers (vide infra).

For further clarification of the coordination geometry, structural modeling was performed to try to classify the coordination geometry of three HFA ligands around metal centers, where the HFA ligands denoted as C are oriented in the same direction in each complex (Figure 5). It should be noted that a precise definition of the sense of chiral arrangement of the three HFA ligands by use of conventional *R*/*S*, *P*/*M*, *A*/*C*, or Λ/Δ

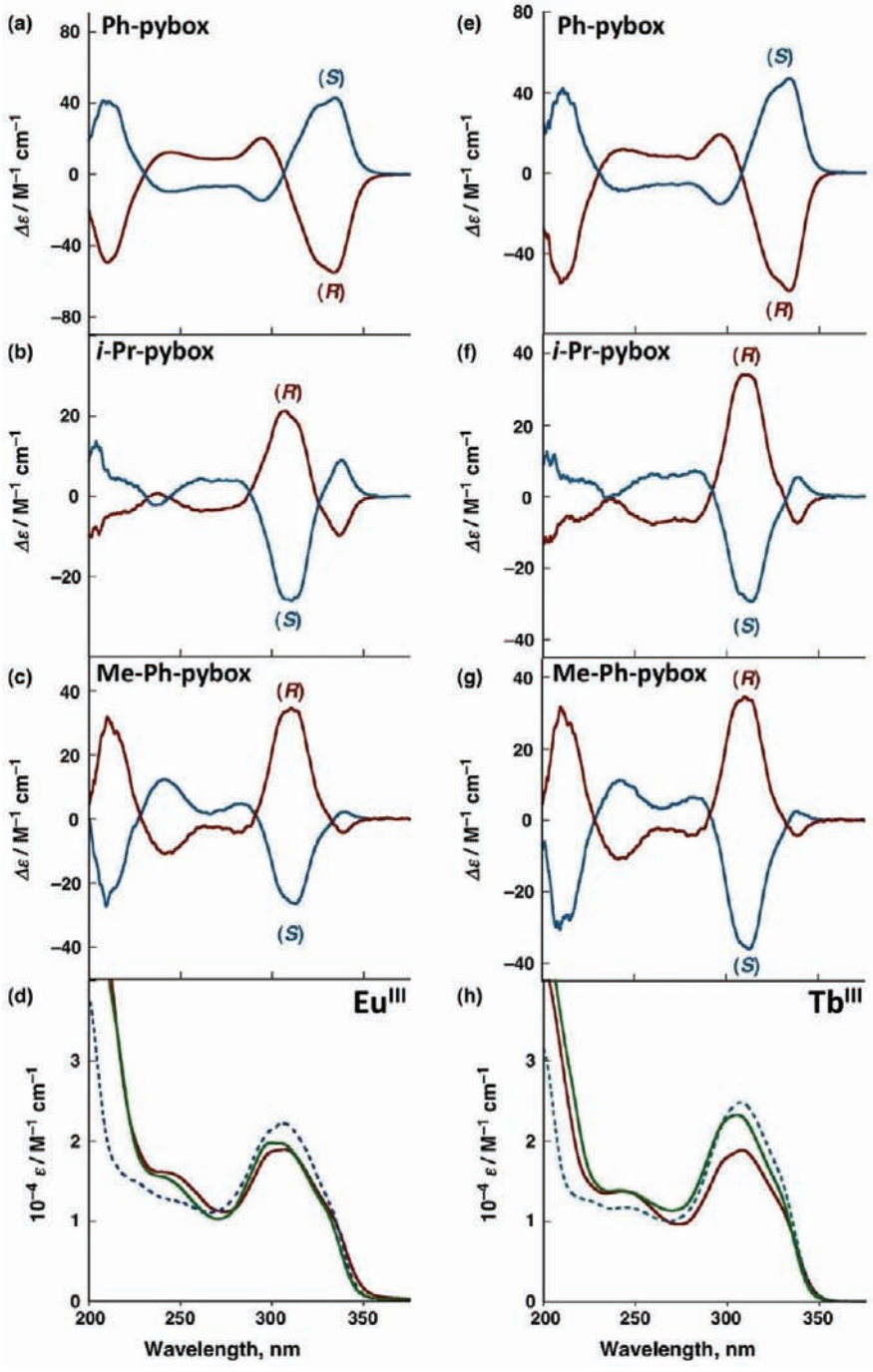

Figure 2. Dark red lines show CD spectra of (a) [(Eu^{III}(*R*)-Ph-pybox)(HFA)$_3$] (4.4×10^{-5} M), (b) [(Eu^{III}(*R*)-*i*-Pr-pybox)(HFA)$_3$] (3.1×10^{-5} M), (c) [(Eu^{III}(*R*)-Me-Ph-pybox)(HFA)$_3$] (2.8×10^{-5} M), (e) [(Tb^{III}(*R*)-Ph-pybox)(HFA)$_3$] (4.4×10^{-5} M), (f) [(Tb^{III}(*R*)-*i*-Pr-pybox)(HFA)$_3$] (3.1×10^{-5} M), and (g) [(Tb^{III}(*R*)-Me-Ph-pybox)(HFA)$_3$] (2.8×10^{-5} M) in CD_3CN at 298 K. Blue lines show those of their optical isomers [(*S*)-isomers]. (d) UV−vis absorption spectra of [(Eu^{III}(*R*)-Ph-pybox)(HFA)$_3$] (dark red solid line), [(Eu^{III}(*R*)-*i*-Pr-pybox)(HFA)$_3$] (blue dashed line), and [(Eu^{III}(*R*)-Me-Ph-pybox)(HFA)$_3$] (green solid line) in CD_3CN at 298 K. (h) UV−vis absorption spectra of [(Tb^{III}(*R*)-Ph-pybox)(HFA)$_3$] (dark red solid line), [(Tb^{III}(*R*)-*i*-Pr-pybox)(HFA)$_3$] (blue dashed line), and [(Tb^{III}(*R*)-Me-Ph-pybox)(HFA)$_3$] (green solid line) in CD_3CN at 298 K.

terminology could be difficult here because of the low symmetry of the HFA coordination sphere. Instead of this, coordination arrangements can be categorized into five typical classes (**I**−**V**) in terms of the dihedral angle formed between HFA planes A and C and that formed between B and C (Figure 5).[48] Coordination arrangements **III** and **IV** are enantiomers of each other; however, they could be identical if one assumes that two HFA ligands (A and B) are the same. The coordination structures of (*R*)- and (*S*)-isomers, [(Eu^{III}(*R*)-*i*-Pr-pybox)(HFA)$_3$] and [(Eu^{III}(*S*)-*i*-Pr-pybox)(HFA)$_3$], are categorized into coordination arrangements **IV** and **III**, respectively (Figure 5). Similarly, core structures of [(Tb^{III}(*R*)-Me-Ph-pybox)(HFA)$_3$] and [(Tb^{III}(*S*)-Me-Ph-pybox)(HFA)$_3$] are classified into **III** and **IV**, respectively (Figure 5). Strong CPL activities of these complexes (Figure1),

dx.doi.org/10.1021/ja201984u |*J. Am. Chem. Soc.* 2011, 133, 9892–9902

Table 2. Crystallographic Parameters and Refinement Details for [(Eu^{III}(*R*)-Ph-pybox)(HFA)$_3$], [(Eu^{III}(*R*)-*i*-Pr-pybox)(HFA)$_3$], [(Eu^{III}(*S*)-*i*-Pr-pybox)(HFA)$_3$], and [(Eu^{III}(*R*)-Me-Ph-pybox)(HFA)$_3$]

	[(Eu^{III}(*R*)-Ph-pybox)(HFA)$_3$]	[(Eu^{III}(*R*)-*i*-Pr-pybox)(HFA)$_3$]	[(Eu^{III}(*S*)-*i*-Pr-pybox)(HFA)$_3$]	[(Eu^{III}(*R*)-Me-Ph-pybox)(HFA)$_3$]
formula sum	$C_{38}H_{22}EuF_{18}N_3O_8$	$C_{32}H_{26}EuF_{18}N_3O_8$	$C_{32}H_{26}EuF_{18}N_3O_8$	$C_{40}H_{26}EuF_{18}N_3O_8$
formula weight	1142.54	1074.50	1074.50	1170.59
crystal system	orthorhombic	monoclinic	monoclinic	orthorhombic
space group	$P2_12_12_1$ (#19)	$P12_11$ (#4)	$P12_11$ (#4)	$P2_12_12_1$ (#19)
a (Å)	12.3639(4)	9.9380(3)	9.9298(2)	11.0802(2)
b (Å)	17.8825(6)	15.7835(5)	15.7715(4)	19.9750(4)
c (Å)	19.2140(7)	13.2164(5)	13.1941(4)	20.2549(4)
α (deg)	90.0000	90.0000	90.0000	90.0000
β (deg)	90.0000	105.4743(9)	105.4737(7)	90.0000
γ (deg)	90.0000	90.0000	90.0000	90.0000
V (Å^3)	4248.2(3)	1997.93(11)	1991.38(8)	4482.96(14)
T (K)	153.1	153.1	153.1	153.1
Z	4	2	2	4
ρ calcd (g·cm^{-3})	1.786	1.786	1.792	1.734
*R*1 [$I > 2\sigma(I)$]	0.0168	0.0275	0.0204	0.0276
*wR*2 [$I > 2\sigma(I)$]	0.0410	0.0713	0.0543	0.0725

Table 3. Crystallographic Parameters and Refinement Details for [(Tb^{III}(*S*)-Ph-pybox)(HFA)$_3$], [(Tb^{III}(*S*)-*i*-Pr-pybox)(HFA)$_3$], [(Tb^{III}(*S*)-Me-Ph-pybox)(HFA)$_3$], and [(Tb^{III}(*R*)-Me-Ph-pybox)(HFA)$_3$]

	[(Tb^{III}(*S*)-Ph-pybox)(HFA)$_3$]	[(Tb^{III}(*S*)-*i*-Pr-pybox)(HFA)$_3$]	[(Tb^{III}(*S*)-Me-Ph-pybox)(HFA)$_3$]	[(Tb^{III}(*R*)-Me-Ph-pybox)(HFA)$_3$]
formula sum	$C_{38}H_{22}TbF_{18}N_3O_8$	$C_{32}H_{26}TbF_{18}N_3O_8$	$C_{40}H_{26}TbF_{18}N_3O_8$	$C_{40}H_{26}TbF_{18}N_3O_8$
formula weight	1149.50	1081.47	1177.56	1177.56
crystal system	orthorhombic	monoclinic	orthorhombic	orthorhombic
space group	$P2_12_12_1$ (#19)	$P12_11$ (#4)	$P2_12_12_1$ (#19)	$P2_12_12_1$ (#19)
a (Å)	12.3065(2)	11.4701(4)	11.0328(2)	11.0743(2)
b (Å)	17.8664(4)	16.2836(5)	19.9521(4)	19.9965(4)
c (Å)	19.1838(4)	12.6644(4)	20.1044(4)	20.1457(4)
α (deg)	90.0000	90.0000	90.0000	90.0000
β (deg)	90.0000	118.1793(8)	90.0000	90.0000
γ (deg)	90.0000	90.0000	90.0000	90.0000
V (Å^3)	4217.99(14)	2085.04(11)	4425.53(14)	4461.20(14)
T (K)	153.1	153.1	153.1	153.1
Z	4	2	4	4
ρ calcd (g·cm^{-3})	1.810	1.722	1.767	1.753
*R*1 [$I > 2\sigma(I)$]	0.0188	0.0421	0.0273	0.0233
*wR*2 [$I > 2\sigma(I)$]	0.0480	0.1141	0.0719	0.0640

therefore, suggest that ligand−ligand interaction between one side arm of the pybox ligand and the HFA ligand (A) contributes to discrimination of two HFA ligands (A and B).

On the other hand, [(Eu^{III}(*R*)-Me-Ph-pybox)(HFA)$_3$] gives almost the same coordination geometry as that of the core structure of [(Eu^{III}(*S*)-*i*-Pr-pybox)(HFA)$_3$] (Figure 5, **III**), but whose CPL and CD spectra are quasi mirror images of each other (Figures 1b,c and 2b,c,respectively). Electric field around the lanthanide(III) metal center has been suggested to be determined mainly by anisotropic ligand polarizability and point charges from the environment atoms.[13−16] This result indicates that anisotropic ligand polarizability largely contributes to the symmetry of electric field around the metal center in this system. Typically in the case of the lanthanide(III) complexes having the Me-Ph-pybox ligand, electronic polarizability of the phenyl ring (neighboring methyl groups) in the Me-Ph-pybox ligand should also contribute to the overall chirality at the metal center.

In the case of [(Tb^{III}(*S*)-*i*-Pr-pybox)(HFA)$_3$], both side arms (*i*-Pr groups) of the pybox ligand have CH/F interactions with the HFA ligands (A and B) [vide supra], inducing a different coordination geometry (**V**) than the other lanthanide(III) complexes (**I**−**IV**). On the other hand, (*R*)-Ph-pybox induces a coordination geometry (**I**) on the core structure of [(Eu^{III}(*R*)-Ph-pybox)(HFA)$_3$], which is an almost mirror image of that of [(Tb^{III}(*S*)-Ph-pybox)(HFA)$_3$] (**II**) [Figure 5]. Coordination structures of **I** and **II** are diastereomers of those of **III**, **IV**, and **V**, in which CD and CPL signals of the lanthanide(III) complexes containing Ph-pybox ligands (corresponding to **I** and **II**) are opposite to those of the lanthanide(III) complexes having the same chirality of *i*-Pr- and Me-Ph-pybox ligands (corresponding to **III**, **IV**, and **V**).

dx.doi.org/10.1021/ja201984u |*J. Am. Chem. Soc.* 2011, 133, 9892–9902

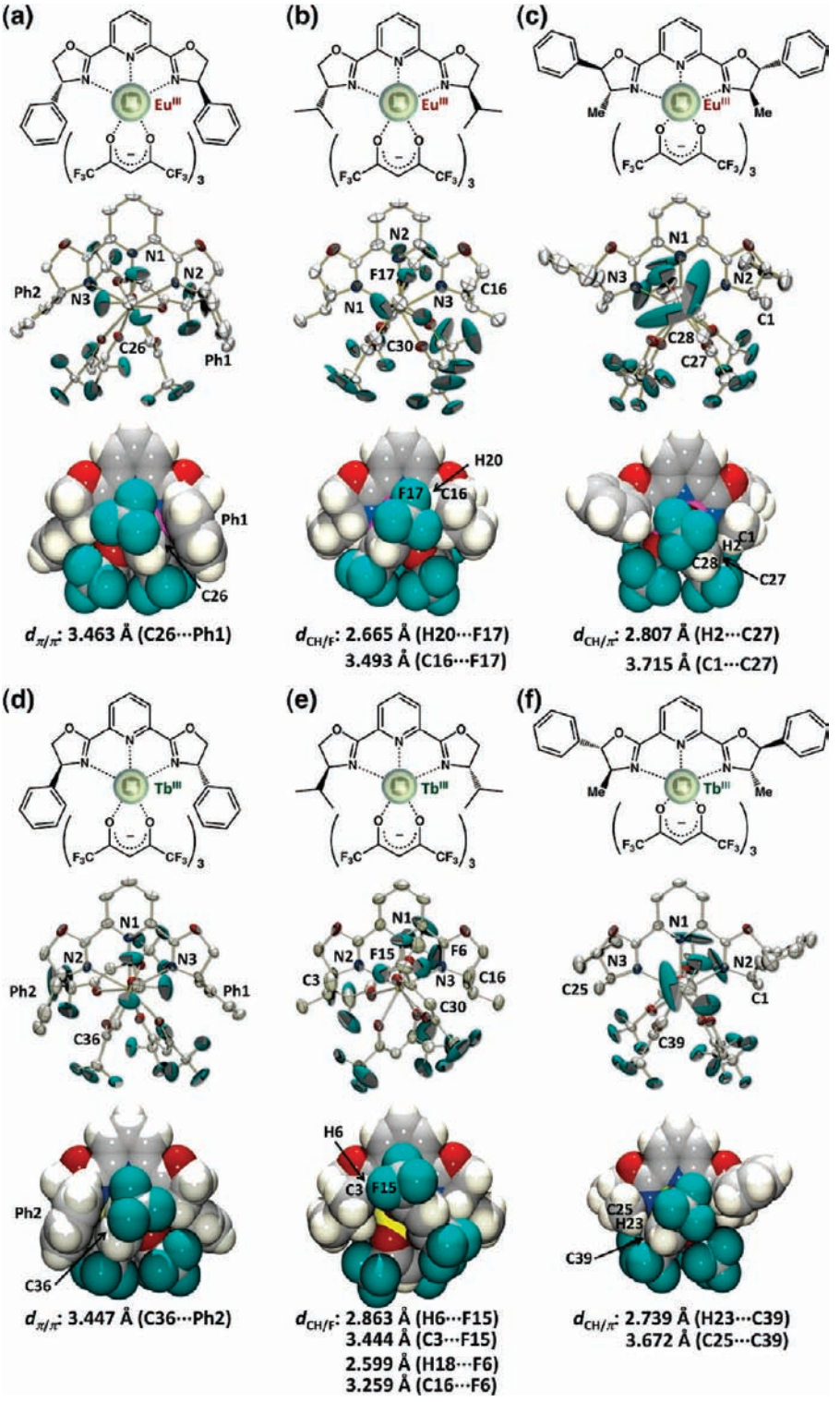

Figure 3. Chemical structures (top) and ORTEP (middle) and space-filling (bottom) views of (a) $[(Eu^{III}(R)\text{-Ph-pybox})(HFA)_3]$, (b) $[(Eu^{III}(R)\text{-}i\text{-Pr-pybox})(HFA)_3]$, (c) $[(Eu^{III}(R)\text{-Me-Ph-pybox})(HFA)_3]$, (d) $[(Tb^{III}(S)\text{-Ph-pybox})(HFA)_3]$, (e) $[(Tb^{III}(S)\text{-}i\text{-Pr-pybox})(HFA)_3]$, and (f) $[(Tb^{III}(S)\text{-Me-Ph-pybox})(HFA)_3]$. $d_{\pi/\pi}$, $d_{CH/F}$, and $d_{CH/\pi}$ are relevant bond lengths in the Eu^{III} and Tb^{III} complexes.

SUMMARY AND CONCLUSIONS

In conclusion, we have demonstrated that the opposite sense of chirality can be obtained for the same chirality of pybox ligands with different side arms in Eu^{III} and Tb^{III} complexes with three achiral HFA ligands. The CPL and CD spectra of $[(Eu^{III}(R)\text{-Ph-pybox})(HFA)_3]$ show quasi mirror images to those of $[(Eu^{III}(R)\text{-}i\text{-Pr-pybox})(HFA)_3]$ and $[(Eu^{III}(R)\text{-Me-Ph-pybox})(HFA)_3]$. Similarly, the $[(Tb^{III}(R)\text{-Ph-pybox})(HFA)_3]$ complex exhibits CPL signals

dx.doi.org/10.1021/ja201984u |*J. Am. Chem. Soc.* 2011, 133, 9892–9902

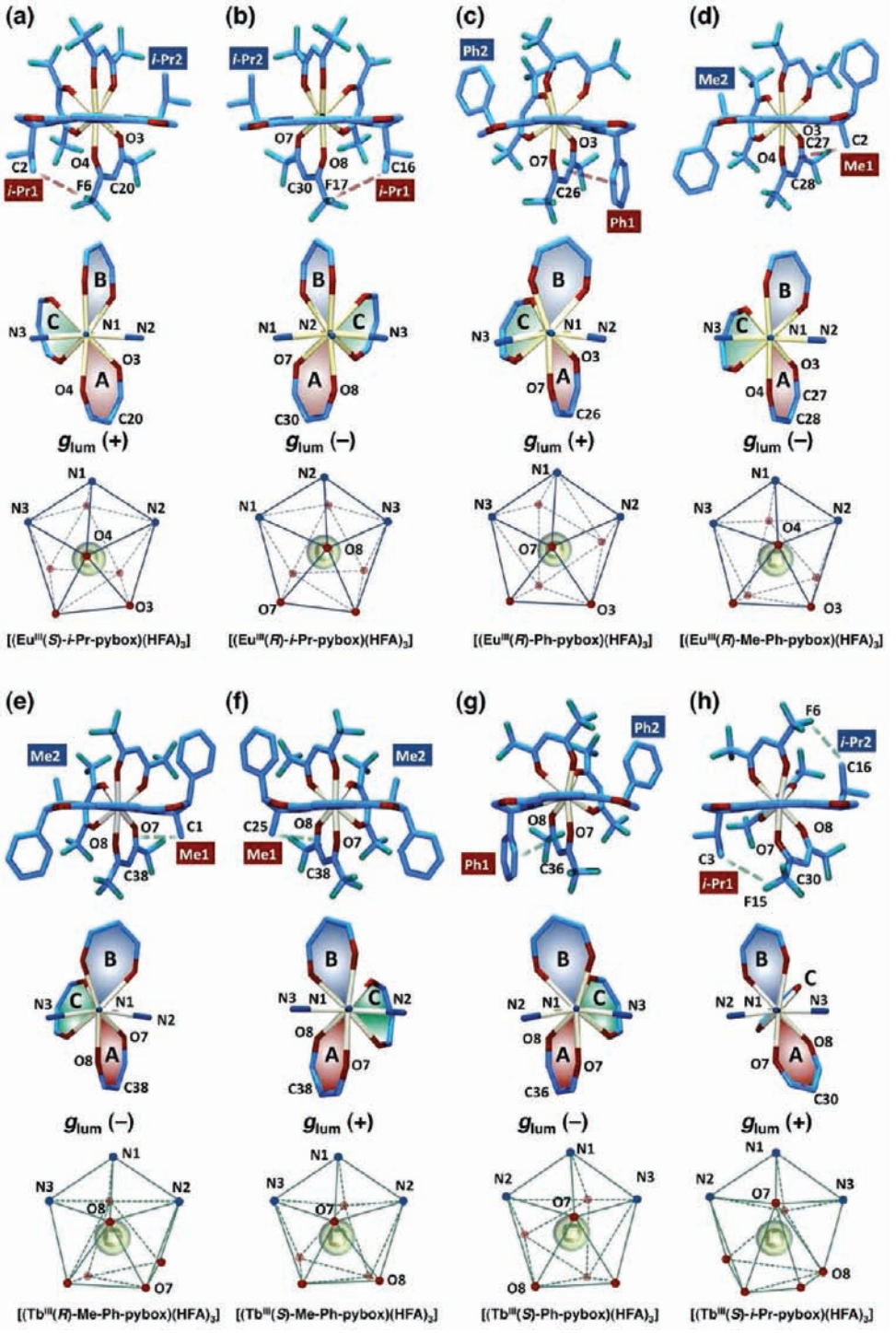

Figure 4. Top views of crystal structures (top) [dashed lines denote ligand−ligand interactions], core structures (middle), and coordination geometries (bottom) of (a) $[(Eu^{III}(S)\text{-}i\text{-Pr-pybox})(HFA)_3]$, (b) $[(Eu^{III}(R)\text{-}i\text{-Pr-pybox})(HFA)_3]$, (c) $[(Eu^{III}(R)\text{-Ph-pybox})(HFA)_3]$, (d) $[(Eu^{III}(R)\text{-Me-Ph-pybox})(HFA)_3]$, (e) $[(Tb^{III}(R)\text{-Me-Ph-pybox})(HFA)_3]$, (f) $[(Tb^{III}(S)\text{-Me-Ph-pybox})(HFA)_3]$, (g) $[(Tb^{III}(S)\text{-Ph-pybox})(HFA)_3]$, and (h) $[(Tb^{III}(S)\text{-}i\text{-Pr-pybox})(HFA)_3]$. Sign of dissymmetry factors of CPL spectra (g_{lum}) at the $^5D_0 \rightarrow {}^7F_1$ transition (Eu^{III} complexes) and the $^5D_4 \rightarrow {}^7F_5$ transition (Tb^{III} complexes) is shown.

almost opposite to those of $[(Tb^{III}(R)\text{-}i\text{-Pr-pybox})(HFA)_3]$ and $[(Tb^{III}(R)\text{-Me-Ph-pybox})(HFA)_3]$ with the same chirality of the pybox ligands. The single-crystal X-ray structural analysis revealed that the asymmetric arrangement around the metal center is primarily determined by the ligand−ligand interactions between the HFA ligand and the chiral pybox ligand, where each pybox ligand has different noncovalent interactions ($\pi-\pi$ stacking, CH/F, and CH/π interactions) with the adjacent HFA ligand. The difference in ligand−ligand interactions alters the sign of CD and CPL signals of the Eu^{III} and Tb^{III} complexes.

dx.doi.org/10.1021/ja201984u | J. Am. Chem. Soc. 2011, 133, 9892–9902

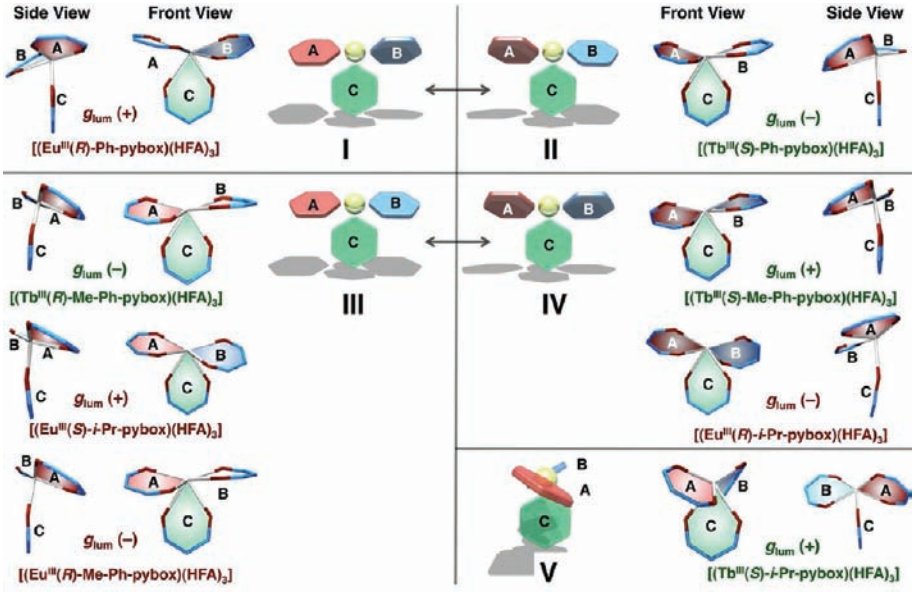

Figure 5. Classification of coordination structures of the HFA ligands in [(Eu^{III}(*R*)-Ph-pybox)(HFA)$_3$], [(Eu^{III}(*R*)-*i*-Pr-pybox)(HFA)$_3$], [(Eu^{III}(*S*)-*i*-Pr-pybox)(HFA)$_3$], [(Eu^{III}(*R*)-Me-Ph-pybox)(HFA)$_3$], [(Tb^{III}(*S*)-Ph-pybox)(HFA)$_3$], [(Tb^{III}(*S*)-*i*-Pr-pybox)(HFA)$_3$], [(Tb^{III}(*S*)-Me-Ph-pybox)-(HFA)$_3$], and [(Tb^{III}(*R*)-Me-Ph-pybox)(HFA)$_3$]. Sign of dissymmetry factors of CPL spectra (g_{lum}) at the $^5D_0 \rightarrow {}^7F_1$ transition (Eu^{III} complexes) and $^5D_4 \rightarrow {}^7F_5$ transition (Tb^{III} complexes) is shown. Arrows denote enantiomer pairs. Definition of the sense of chiral arrangement of HFA ligands: **I**, dihedral angle between A and C < 90° and between B and C > 90°; **II**, dihedral angle between A and C > 90° and between B and C < 90°; **III**, dihedral angle between A and C < 90° and between B and C < 90°; **IV**, dihedral angle between A and C > 90° and between B and C > 90°; **V**, the other coordination arrangement.

■ ASSOCIATED CONTENT

Ⓢ Supporting Information. One scheme diagramming our CPL measurement system and five figures showing emission decay profiles of the Eu^{III} complexes, temperature dependence of emission intensities of the Eu^{III} and Tb^{III} complexes, CD spectra at the absorption bands from the 4f−4f transitions, solid-state CD spectra, and ^{1}H,^{1}H COSY NMR spectrum of [(Eu^{III}(*R*)-Ph-pybox)(HFA)$_3$]. This material is available free of charge via the Internet at http://pubs.acs.org.

■ AUTHOR INFORMATION

Corresponding Author

yuasaj@ms.naist.jp; tkawai@ms.naist.jp

Present Addresses

[†]Division of Materials Chemistry, Faculty and Graduate School of Engineering, Hokkaido University, N13 W8, Kita-ku, Sapporo 060-8628, Japan.

■ ACKNOWLEDGMENT

This work was partially supported by Grants-in-Aid (21750147 and 21107520) from the Ministry of Education, Culture, Sports, Science and Technology, Japan. This paper was improved through the suggestions and comments of Professor Leigh McDowell (Nara Institute of Science and Technology). Professor Tsuyoshi Kawai also thanks for financial support from the project for Development of Systems and Technology for advanced Measurements and Analysis from Japan Science and Technology Agency, JST.

■ REFERENCES

(1) (a) Johnson, J. S.; Evans, D. A. *Acc. Chem. Res.* **2000**, *33*, 325. (b) Evans, D. A.; Johnson, J. S. In *Comprehensive Asymmetric Catalysis*; Jacobsen, E. N., Pfaltz, A., Yamamoto, H., Eds.; Springer Verlag: Heidelberg, Germany, 1999; Vol. 3, pp 1178−1235.

(2) (a) Rasappan, R.; Laventine, D.; Reiser, O. *Coord. Chem. Rev.* **2008**, *252*, 702. (b) Corminboeuf, O.; Quaranta, L.; Renaud, P.; Liu, M.; Jasperse, C. P.; Sibi, M. P. *Chem.−Eur. J.* **2003**, *9*, 28. (c) Quaranta, L.; Corminboeuf, O.; Renaud, P. *Org. Lett.* **2002**, *4*, 39. (d) Alvarez, S.; Schefzick, S.; Lipkowitz, K.; Avnir, D. *Chem.−Eur. J.* **2003**, *9*, 5832. (e) García, J. I.; Jiménez-Osés, G.; Martínez-Merino, V.; Mayoral, J. A.; Pires, E.; Villalba, I. *Chem.−Eur. J.* **2007**, *13*, 4064.

(3) (a) Donoghue, P. J.; Helquist, P.; Norrby, P.-O.; Wiest, O. *J. Am. Chem. Soc.* **2009**, *131*, 410. (b) Gridnev, I. D.; Higashi, N.; Asakura, K.; Imamoto, T. *J. Am. Chem. Soc.* **2000**, *122*, 7183. (c) Gridnev, I. D.; Imamoto, T. *Acc. Chem. Res.* **2004**, *37*, 633. (d) Hoge, G.; Wu, H.-P.; Kissel, W. S.; Pflum, D. A.; Greene, D. J.; Bao, J. *J. Am. Chem. Soc.* **2004**, *126*, 5966.

(4) Corey, E. J. *Angew. Chem., Int. Ed.* **2002**, *41*, 1650.

(5) Crassous, J. *Chem. Soc. Rev.* **2009**, *38*, 830.

(6) Tsukube, H.; Shinoda, S. *Chem. Rev.* **2002**, *102*, 2389.

(7) (a) Montgomery, C. P.; New, E. J.; Parker, D.; Peacock, R. D. *Chem. Commun.* **2008**, 4261. (b) Yu, J. H.; Parker, D.; Pal, R.; Poole, R. A.; Cann, M. J. *J. Am. Chem. Soc.* **2006**, *128*, 2294. (c) New, E. J.; Parker, D.; Smith, D. G.; Walton, J. W. *Curr. Opin. Chem. Biol.* **2010**, *14*, 238. (d) Montgomery, C. P.; Murray, B. S.; New, E. J.; Pal, R.; Parker, D. *Acc. Chem. Res.* **2009**, *42*, 925.

(8) (a) Coruh, N.; Riehl, J. P. *Biochemistry* **1992**, *31*, 7970. (b) Rexwinkel, R. B.; Meskers, S. C. J.; Riehl, J. P.; Dekkers, H. P. J. M. *J. Phys. Chem.* **1992**, *96*, 1112. (c) Meskers, S. C. J.; Dekkers, H. P. J. M. *J. Phys. Chem. A* **2001**, *105*, 4589. (d) Meskers, S. C. J.; Dekkers, H. P. J. M.; Rapenne, G.; Sauvage, J.-P. *Chem.−Eur. J.* **2000**, *6*, 2129. (e) Meskers, S. C. J.; Dekkers, H. P. J. M. *J. Am. Chem. Soc.* **1998**, *120*, 6413. (f) Cisnetti, F.; Gateau, C.; Lebrun, C.; Delangle, P. *Chem.−Eur. J.* **2009**, *15*, 7456.

(9) (a) Knof, U.; von Zelewsky, A. *Angew. Chem., Int. Ed.* **1999**, *38*, 302. (b) Bark, T.; Düggeli, M.; Stoeckli-Evans, H.; von Zelewsky, A. *Angew. Chem., Int. Ed.* **2001**, *40*, 2848.

(10) Knight, P. D.; Scott, P. *Coord. Chem. Rev.* **2003**, *242*, 125.
(11) (a) Mamula, O.; von Zelewsky, A. *Coord. Chem. Rev.* **2003**, *242*, 87. (b) Mamula, O.; Von Zelewsky, A.; Bark, T.; Stoeckli-Evans, H.; Neels, A.; Bernardinelli, G. *Chem.—Eur. J.* **2000**, *6*, 3575. (c) Hayoz, P.; von Zelewsky, A.; Stoeckli-Evans, H. *J. Am. Chem. Soc.* **1993**, *115*, 5111.
(12) (a) Garcia, L.; Maisonneuve, S.; Xie, J.; Guillot, R.; Dorlet, P.; Riviére, E.; Desmadril, M.; Lambert, F.; Policar, C. *Inorg. Chem.* **2010**, *49*, 7282. (b) Ahn, D.-R.; Kim, T. W.; Hong, J.-I. *J. Org. Chem.* **2001**, *66*, 5008.
(13) (a) Richardson, F. S.; Riehl, J. P. *Chem. Rev.* **1977**, *77*, 773. (b) Riehl, J. P.; Richardson, F. S. *Chem. Rev.* **1986**, *86*, 1.
(14) Riehl, J. P. Muller, G. . In *Handbook on the Physics and Chemistry of Rare Earths*; Gschneidner, K. A., Jr., Bünzli, J.-C. G. Pecharsky, V. K., Eds.; North Holland Publishing Company: Amsterdam, 2005; Vol. 34, Chapt. 220, pp 289−357.
(15) (a) Muller, G. *Dalton Trans.* **2009**, 9692. (b) Parker, D.; Dickins, R. S.; Puschmann, H.; Crossland, C.; Howard, J. A. *Chem. Rev.* **2002**, *102*, 1977. (c) dos Santos, C. M. G.; Harte, A. J.; Quinn, S. J.; Gunnlaugsson, T. *Coord. Chem. Rev.* **2008**, *252*, 2512. (d) Bünzli, J.-C. G.; Piguet, C. *Chem. Soc. Rev.* **2005**, *34*, 1048.
(16) Richardson, F. S. *Inorg. Chem.* **1980**, *19*, 2806.
(17) (a) Gregoliński, J.; Lisowski, J. *Angew. Chem., Int. Ed.* **2006**, *45*, 6122. (b) Gregoliński, J.; Starynowicz, P.; Hua, K. T.; Lunkley, J. L.; Muller, G.; Lisowski, J. *J. Am. Chem. Soc.* **2008**, *130*, 17761. (c) Lunkley, J. L.; Shirotani, D.; Yamanari, K.; Kaizaki, S.; Muller, G. *J. Am. Chem. Soc.* **2008**, *130*, 13814. (d) Bonsall, S. D.; Houcheime, M.; Straus, D. A.; Muller, G. *Chem. Commun.* **2007**, *35*, 3676.
(18) (a) Dickins, R. S.; Howard, J. A. K.; Maupin, C. L.; Moloney, J. M.; Parker, D.; Riehl, J. P.; Siligardi, G.; Williams, J. A. G. *Chem.—Eur. J.* **1999**, *5*, 1095. (b) Abdollahi, S.; Harris, W. R.; Riehl, J. P. *J. Phys. Chem.* **1996**, *100*, 1950. (c) Maupin, C. L.; Dickins, R. S.; Govenlock, L. G.; Mathieu, C. E.; Parker, D.; Williams, J. A. G.; Riehl, J. P. *J. Phys. Chem. A* **2000**, *104*, 6709. (d) Cantuel, M.; Bernaldielli, G.; Muller, G.; Riehl, J. P.; Piguet, C. *Inorg. Chem.* **2004**, *43*, 1840.
(19) (a) Bruce, J. I.; Dickins, R. S.; Govenlock, L. J.; Gunnlaugsson, T.; Lopinski, S.; Lowe, M. P.; Parker, D.; Peacock, R. D.; Perry, J. J. B.; Aime, S.; Botta, M. *J. Am. Chem. Soc.* **2000**, *122*, 9674. (b) Leonard, J. P.; Jensen, P.; McCabe, T.; O'Brien, J. E.; Peacock, R. D.; Kruger, P. E.; Gunnlaugsson, T. *J. Am. Chem. Soc.* **2007**, *129*, 10986. (c) Murray, B. S.; Parker, D.; dos Santos, C. M. G.; Peacock, R. D. *Eur. J. Inorg. Chem.* **2010**, 2663.
(20) (a) Mamula, O.; Lama, M.; Telfer, S. G.; Nakamura, A.; Kuroda, R.; Stoeckli-Evans, H.; Scopelitti, R. *Angew. Chem., Int. Ed.* **2005**, *44*, 2527. (b) Lama, M.; Mamula, O.; Kottas, G. S.; Rizzo, F.; De Cola, L.; Nakamura, A.; Kuroda, R.; Stoeckli-Evans, H. *Chem.—Eur. J.* **2007**, *13*, 7358.
(21) (a) Seitz, M.; Moore, E. G.; Ingram, A. J.; Muller, G.; Raymond, K. N. *J. Am. Chem. Soc.* **2007**, *129*, 15468. (b) Moore, E. G.; Samuel, A. P. S.; Raymond, K. N. *Acc. Chem. Res.* **2009**, *42*, 542. (c) Petoud, S.; Muller, G.; Moore, E. G.; Xu, J.; Sokolnicki, J.; Riehl, J. P.; Le, U. N.; Cohen, S. M.; Raymond, K. N. *J. Am. Chem. Soc.* **2007**, *129*, 77. (d) D'Aléo, A.; Xu, J.; Do, K.; Muller, G.; Raymond, K. N. *Helv. Chim. Acta* **2009**, *92*, 2439. (e) Seitz, M.; Do, K.; Ingram, A. J.; Moore, E. G.; Muller, G.; Raymond, K. N. *Inorg. Chem.* **2009**, *48*, 8469. (f) Samuel, A. P. S.; Lunkley, J. L.; Muller, G.; Raymond, K. N. *Eur. J. Inorg. Chem.* **2010**, 3343.
(22) (a) Richardson, F. S.; Brittain, H. G. *J. Am. Chem. Soc.* **1981**, *103*, 18. (b) Luk, C. K.; Richardson, F. S. *J. Am. Chem. Soc.* **1975**, *97*, 6666. (c) Brittain, H. G.; Richardson, F. S. *J. Am. Chem. Soc.* **1976**, *98*, 5858. (d) Brittain, H.; Richardson, F. S. *J. Am. Chem. Soc.* **1977**, *99*, 65. (e) Brittain, H. G.; Pearson, K. H. *Inorg. Chem.* **1983**, *22*, 78. (f) Yang, X.; Brittain, H. G. *Inorg. Chem.* **1981**, *20*, 4273. (g) Brittain, H. G.; Johnson, C. R. *Inorg. Chem.* **1985**, *24*, 4465.
(23) Harada, T.; Nakano, Y.; Fujiki, M.; Naito, M.; Kawai, T.; Hasegawa, Y. *Inorg. Chem.* **2009**, *48*, 11242.
(24) For circularly polarized luminescence studies of transition metal complexes, see (a) Schaffner-Hamann, C.; von Zelewsky, A.; Barbieri, A.; Barigelletti, F.; Muller, G.; Riehl, J. P.; Neels, A. *J. Am. Chem. Soc.* **2004**, *126*, 9339. (b) Oyler, K. D.; Coughlin, F. J.; Bernhard, S. *J. Am. Chem. Soc.* **2007**, *129*, 210. (c) Coughlin, F. J.; Westrol, M. S.; Oyler, K. D.; Byme, N.; Kraml, C.; Zysman-Colman, E.; Lowry, M. S.; Bernhard, S. *Inorg. Chem.* **2008**, *47*, 2039. (d) Gunde, K. E.; Credi, A.; Jandrasics, E.; von Zelewsky, A.; Richardson, F. S. *Inorg. Chem.* **1997**, *36*, 426.
(25) Richardson et al. provided a detailed theory for optical activity of the f−f transitions in lanthanide(III) complexes. See Richardson, F. S.; Faulkner, T. R. *J. Chem. Phys.* **1982**, *76*, 1595.
(26) For selected examples of chiral lanthanide(III) catalysis containing a bis(oxazoline) ligand, see (a) Evans, D. A.; Wu, J. *J. Am. Chem. Soc.* **2003**, *125*, 10162. (b) Evans, D. A.; Fandrick, K. R.; Song, H.-J.; Scheidt, K. A.; Xu, R. *J. Am. Chem. Soc.* **2007**, *129*, 10029. (c) Evans, D. A.; Fandrick, K. R.; Song, H.-J. *J. Am. Chem. Soc.* **2005**, *127*, 8942. (d) Evans, D. A.; Scheidt, K. A.; Fandrick, K. R.; Lam, H. W.; Wu, J. *J. Am. Chem. Soc.* **2003**, *125*, 10780. (e) Evans, D. A.; Sweeney, Z. K.; Rovis, T.; Tedrow, J. S. *J. Am. Chem. Soc.* **2001**, *123*, 12095.
(27) For recent reports on emission and CPL studies of lanthanide(III) complexes with bis(oxazoline) ligands, see (a) Bozoklu, G.; Marchal, C.; Gateau, C.; Pécaut, J.; Imbert, D.; Mazzanti, M. *Chem.—Eur. J.* **2010**, *16*, 6159. (b) Matsumoto, K.; Suzuki, K.; Tsukuda, T.; Tsubomura, T. *Inorg. Chem.* **2010**, *49*, 4717. (c) de Bettencourt-Dias, A. *J. Am. Chem. Soc.* **2007**, *129*, 15436.
(28) (a) Hasegawa, Y.; Kimura, Y.; Murakoshi, K.; Wada, Y.; Yamanaka, T.; Kim, J.; Nakashima, N.; Yanagida, S. *J. Phys. Chem.* **1996**, *100*, 10201. (b) Hasegawa, Y.; Murakoshi, K.; Wada, Y.; Yanagida, S.; Kim, J.; Nakashima, N.; Yamanaka, T. *Chem. Phys. Lett.* **1996**, *248*, 8. (c) Nakamura, K.; Hasegawa, Y.; Kawai, H.; Yasuda, N.; Kanehisa, N.; Kai, Y.; Nagamura, T.; Yanagida, S.; Wada, Y. *J. Phys. Chem. A* **2007**, *111*, 3029. (d) Hasegawa, Y.; Tsuruoka, S.; Yoshida, T.; Kawai, H.; Kawai, T. *J. Phys. Chem. A* **2008**, *112*, 803.
(29) (a) Chauvin, A.-S.; Gumy, F.; Matsubayashi, I.; Hasegawa, Y.; Bünzli, J.-C. G. *Eur. J. Inorg. Chem.* **2006**, 473. (b) Eliseeva, S. V.; Ryazanov, M.; Gumy, F.; Troyanov, S. I.; Lepenev, L. S.; Bünzli, J.-C. G.; Kuzmina, N. P. *Eur. J. Inorg. Chem.* **2006**, 4809.
(30) A part of the preliminary results on CPL spectrum of the single crystal of $[(Eu^{III}(R)\text{-Ph-pybox})(HFA)_3]$ using our CPL measurement system has appeared. See Tsumatori, H.; Harada, T.; Yuasa, J.; Hasegawa, Y.; Kawai, T. *Appl. Phys. Express* **2011**, *4*, No. 011601.
(31) The deuterated solvent (CD_3CN) was used in emission and CPL measurements to suppress the nonradiative transition through vibrational relaxation processes.
(32) Bünzli, J.-C. G. *Chem. Rev.* **2010**, *110*, 2729.
(33) (a) Katagiri, S.; Hasegawa, Y.; Wada, Y.; Yanagida, S. *Chem. Lett.* **2004**, *33*, 1438. (b) Katagiri, S.; Hasegawa, Y.; Wada, Y.; Mitsuo, K.; Yanagida, S. *J. Alloys Compd.* **2006**, *408−412*, 809. (c) Katagiri, S.; Tsukahara, Y.; Hasegawa, Y.; Wada, Y. *Bull. Chem. Soc. Jpn.* **2007**, *80*, 1492.
(34) (a) Yu, J.-a. *J. Lumin.* **1998**, *78*, 265. (b) Gutierrez, F.; Tedeschi, C.; Maron, L.; Daudey, J.-P.; Poteau, R.; Azema, J.; Tisnes, P.; Picard, C. *Dalton Trans.* **2004**, 1334.
(35) Sato, S.; Wada, M. *Bull. Chem. Soc. Jpn.* **1970**, *43*, 1955.
(36) Weak CD peaks of $[(Eu^{III}(R)\text{-Ph-pybox})(HFA)_3]$ at 465 and 525 nm due to the $^7F_0 \rightarrow {}^5D_2$ and $^7F_0 \rightarrow {}^5D_1$ transitions in Eu^{III} ions also show a quasi mirror image of the CD patterns of $[(Eu^{III}(R)\text{-}i\text{-Pr-pybox})(HFA)_3]$ and $[(Eu^{III}(R)\text{-Me-Ph-pybox})(HFA)_3]$ (see Supporting Information, Figure S4).
(37) Telfer et al. reported detailed theoretical studies focusing on Cotton effects in CD spectra result from excitonic couplings between the coordinated ligands. See (a) Telfer, S. G.; Tajima, N.; Kuroda, R.; Cantuel, M.; Piguet, C. *Inorg. Chem.* **2004**, *43*, 5302. (b) Telfer, S. G.; Tajima, N.; Kuroda, R. *J. Am. Chem. Soc.* **2004**, *126*, 1408. (c) Telfer, S. G.; Kuroda, R.; Sato, T. *Chem. Commun.* **2003**, 1064.
(38) Strong Cotton effects in observed CD spectra (Figure 2) of the Eu^{III} and Tb^{III} complexes may result from some excitonic couplings between three HFA ligands around the metal center.
(39) (a) Shirotani, D.; Suzuki, T.; Kaizaki, S. *Inorg. Chem.* **2006**, *45*, 6111. (b) Liu, X.-G.; Zhou, K.; Dong, J.; Zhu, C.-J.; Bao, S.-S.; Zheng, L.-M. *Inorg. Chem.* **2009**, *48*, 1901.

(40) Solid-state CD spectra of [(Tb^{III}(*R*/*S*)-Ph-pybox)(HFA)$_3$] and [(Tb^{III}(*R*/*S*)-*i*-Pr-pybox)(HFA)$_3$] show similar CD profiles to those obtained in solution (Figure 2e,f; see also Supporting Information, Figure S5).

(41) Although the space groups of [(Eu^{III}(*R*)-*i*-Pr-pybox)(HFA)$_3$] and [(Tb^{III}(*S*)-*i*-Pr-pybox)(HFA)$_3$] ($P12_11$) are different from those of the other lanthanide(III) complexes ($P2_12_12_1$), the difference in space group could not be responsible for the inversion of CD and CPL signals of the complexes in solution (Figures 1 and 2).

(42) The CH/F interaction (H6···F15) in [(Tb^{III}(*S*)-*i*-Pr-pybox)-(HFA)$_3$] makes the pyridine ring of *i*-Pr-pybox lie close to F13 (neighboring F15) of the HFA ligand (d = 3.529 Å).

(43) (a) Di Bari, L.; Pescitelli, G.; Sherry, A. D.; Woods, M. *Inorg. Chem.* **2005**, *44*, 8391. (b) Di Bari, L.; Salvadori, P. *Coord. Chem. Rev.* **2005**, *249*, 2854.

(44) Lennartson, A.; Vestergren, M.; Hakansson, M. *Chem.—Eur. J.* **2005**, *11*, 1757.

(45) Brittain, H. G. *Inorg. Chem.* **1980**, *19*, 2233.

(46) Although ligand−ligand interactions between the pybox ligands and the HFA ligands differentiate two Ph groups of [(Eu^{III}(*R*)-Ph-pybox)(HFA)$_3$] in the X-ray crystal structure (Figure 3a), ^{1}H NMR spectrum of [(Eu^{III}(*R*)-Ph-pybox)(HFA)$_3$] shows symmetrical patterns (see Supporting Information, Figure S6), indicating rapid exchange between the individual Ph groups on the NMR time scale.

(47) In the case of [(Eu^{III}(*R*)-Me-Ph-pybox)(HFA)$_3$] (Figure 3c), although the distance between Me-2 and the other HFA ligand (B) [corresponding H_{22}···C_{34} distance of 2.902 Å] indicates somewhat weak interaction between them, which is not comparable to CH/F interaction between Me-1 and the HFA ligand (A) [H2···C27 distance of 2.807 Å]. In the case of [(Tb^{III}(*S*)-Me-Ph-pybox)(HFA)$_3$] (Figure 3f), however, there are apparent CH/π interactions between Me-1 and the HFA ligand (A) [H6···F15 distance of 2.863 Å] as well as Me-1 and the HFA ligand (B) [H18···F6 distance of 2.599 Å].

(48) Although one may think that other possible definitions of the sense of chiral arrangement of HFA ligands are possible, the core structures of the lanthanide(III) complexes examined here could be classified into five typical classes using any definition.